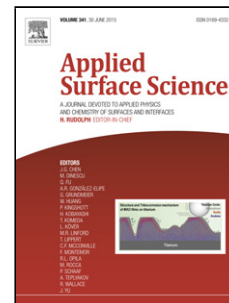


Accepted Manuscript

Title: GRAPHITE INTERCALATED POLYANILINE COMPOSITE WITH SUPERIOR ANTICORROSIVE AND HYDROPHOBIC PROPERTIES, AS PROTECTIVE COATING MATERIAL ON STEEL SURFACES

Authors: R.M.N.M. Rathnayake, M.M.M.G.P.G. Mantilaka, Masanori Hara, Hsin-Hui Huang, H.W.M.A.C. Wijayasinghe, Masamichi Yoshimura, H.M.T.G.A. Pitawala



PII: S0169-4332(17)30777-8
DOI: <http://dx.doi.org/doi:10.1016/j.apsusc.2017.03.119>
Reference: APSUSC 35495

To appear in: *APSUSC*

Received date: 2-12-2016
Revised date: 24-2-2017
Accepted date: 13-3-2017

Please cite this article as: R.M.N.M.Rathnayake, M.M.M.G.P.G.Mantilaka, Masanori Hara, Hsin-Hui Huang, H.W.M.A.C.Wijayasinghe, Masamichi Yoshimura, H.M.T.G.A.Pitawala, GRAPHITE INTERCALATED POLYANILINE COMPOSITE WITH SUPERIOR ANTICORROSIVE AND HYDROPHOBIC PROPERTIES, AS PROTECTIVE COATING MATERIAL ON STEEL SURFACES, *Applied Surface Science* <http://dx.doi.org/10.1016/j.apsusc.2017.03.119>

This is a PDF file of an unedited manuscript that has been accepted for publication. As a service to our customers we are providing this early version of the manuscript. The manuscript will undergo copyediting, typesetting, and review of the resulting proof before it is published in its final form. Please note that during the production process errors may be discovered which could affect the content, and all legal disclaimers that apply to the journal pertain.

<AT>GRAPHITE INTERCALATED POLYANILINE COMPOSITE WITH SUPERIOR ANTICORROSIVE AND HYDROPHOBIC PROPERTIES, AS PROTECTIVE COATING MATERIAL ON STEEL SURFACES

<AU>R.M.N.M. Rathnayake^{a,c}, M.M.M.G.P.G. Mantilaka^b, Masanori Hara^c, Hsin-Hui Huang^c, H.W.M.A.C. Wijayasinghe^{a*} [Email:athula@ifs.ac.lk](mailto:athula@ifs.ac.lk), Masamichi Yoshimura^c, H.M.T.G.A. Pitawala^d

<AFF>^aNational Institute of Fundamental Studies, Kandy, Sri Lanka

<AFF>^bSri Lanka Institute of Nanotechnology, Nanotechnology and Science Park, Mahenwatte, Pitipana, Homagama, Sri Lanka

<AFF>^cGraduate School of Engineering, Toyota Technological Institute, 2-12-1 Hisakata, Tempaku, Nagoya 468-8511, Japan

<AFF>^dDepartment of Geology, University of Peradeniya, Peradeniya, Sri Lanka

<PA>National Institute of Fundamental Studies, Hanatana Road, Kandy, Sri Lanka.

<ABS-Head><ABS-HEAD>Graphical abstract

<ABS-P>

<ABS-P><xps:span class="xps_Image">fx1</xps:span>

<ABS-HEAD>Highlights ► In this paper, it has been utilized a novel method to prepare a new composite material of PANI/NPG graphite composite, using NPG vein graphite variety. ► It is found that the composite works as an anti-corrosive coating on steel surfaces. Further, the prepared composite shows good hydrophobic ability, which is very useful in preventing corrosion on metal surfaces. ► The prepared PANI/NPG composite material shows a significantly high corrosion resistance compared to alkyd resin/PANI coatings or alkyd resin coatings, on steel surfaces.

<ABS-HEAD>Abstract

<ABS-P>Solid polymer composite systems are widely being used for potential technological applications in secondary energy sources and electrochromic devices. In this study, we synthesized and characterized a composite material composed of polyaniline (PANI) and natural needle platy (NPG) vein graphite. Fourier transform infrared spectroscopy (FTIR), X-ray diffraction (XRD), cyclic voltammetry (CV), scanning electron microscopy (SEM), X-ray photoelectron spectroscopy (XPS), micro-Raman analysis, thermogravimetric and differential thermal analysis (TGA/DTA), transmission electron microscopy (TEM) were used to study the structural and electrochemical properties of the prepared PANI/NPG graphite composite. XPS, FTIR, and micro-Raman analysis confirmed the existence of relevant functional groups and bonding in the prepared PANI/NPG composite material. The composite shows a very low corrosion rate, approximately 29 μm per year, and high hydrophobicity on steel surfaces, which helps to prevent the corrosion due to O_2 penetration towards the metal surface. It indicates that the composite can be used as a high potential surface coating material to anticorrosion. The specific capacitance of PANI/NPG composite is 833.3 F g^{-1} , which is higher than that of PANI. This synergistic electrical performance result proves the prepared PANI/NPG graphite composite as a suitable protective coating material for steel surfaces.

<KWD>Keywords: PANI/NPG composite; anticorrosion; steel surface; hydrophobicity

<H1>1. Introduction

Intrinsically conducting polymers (ICPs) have become a landmark for new research innovations due to their interesting chemical, physical and electrical properties [1]. Electrical and electrochemical properties of ICPs have been remarkably enhanced through the incorporation of carbonaceous materials such as natural graphite, carbon foam, carbon nanotubes etc. [2-4]. Graphite and polyaniline (PANI) have shown greater electrical properties in their composite materials for this purpose [5]. Furthermore, polymer composites represent radical alternatives to the conventional filled polymers or polymer blends due to the synergetic properties. Polymer composites are mainly studied for their use as conducting or non-conducting polymers, based on the purpose of their application. Polyaniline (PANI) is one of the intensively studied electrically conducting polymers that belongs to the semi-flexible rod polymer family [6-8]. Alternatively, composite materials containing components of phyllosilicate-type minerals and a conducting polymer have been synthesized by polymerizing the respective monomer in the presence of colloidal mineral suspension[8]. The colour of polyaniline depends on its oxidation states and they can be used in sensors and electrochromic devices [9]. Treatment of emeraldine salt form of PANI with acids was reported to increase the electrical conductivity by ten orders of magnitude [10]. Polyaniline is attractive because it is relatively inexpensive. It has three distinct oxidation states with different colours and possesses an acid/base doping properties. Some of the attractive fields for current and potential applications of polyaniline are in antistatic, charge dissipation or electrostatic dispersive (ESD) coatings and blends, electromagnetic interference shielding (EMI) and anticorrosive coatings [11-14]. This approach of preparing PANI/graphite composite is very important to develop the surface coating industry [15, 16]. Specifically, our study explored the use of the natural needle platy (NPG) vein graphite as a base dispersant to develop a new PANI/NPG composite material. This NPG vein graphite has 99 % purity at their initial stage. Graphite is very attractive material due to its moderate electrical and thermal conductivity, self-lubricating ability and very high melting temperature above 3600°C [17]. In addition, vein graphite is a cheaper naturally occurring mineral with very high crystallinity and natural purity. Therefore, graphite has been used as a conductive additive to improve the conductivity of polymer materials [5, 18-20].

In this paper, we utilized a novel method to prepare a new composite material of PANI/NPG graphite composite, using natural NPG vein graphite variety. It is expected this new composite to be developed as an anticorrosive and hydrophobic protective coating on steel surfaces. This initiation is important in developing natural vein graphite based products for surface coating industry. The novelty of this study is the preparation of a new composite material as a hydrophobic and anticorrosive coating for steel bars, by using the inherent properties of high purity and highly crystallinity of natural NPG vein graphite.

<H1>2. Experimental Design

<H2>2.1 Materials

Aniline (99.5%), sodium persulfate (99.9%) and hydrochloric acid (36.5%) were purchased from the Sigma-Aldrich. Analytical grade ethanol (99.8%) and magnesium chloride (99.0%) were purchased from the VWR. Freshly distilled aniline was used for the experiment. Needle platy graphite (NPG) variety of natural vein graphite of Sri Lankan origin, was also used. The obtained NPG raw graphite was purified using the

acid leach method and the purity was upgraded up to 99% before using for this study.

<H2>2.2 Preparation of PANI/graphite composite

For the preparation of the PANI/NPG graphite composite, 25 ml of H₂O and 25 ml of 1.5 M HCl were added to 2 g of purified NPG graphite contained in a glass beaker and stirred using a magnetic stirrer until the mixture became homogeneous. Then 2 ml of aniline was added to the same mixture and stirred for another 30 minutes. After that, 25 ml of 0.4 M (NH₄)₂S₂O₈ was added dropwise into the mixture at the rate of 0.05 ml s⁻¹. Finally, the prepared composite material was thoroughly washed with 200 ml of distilled water and dried in a vacuum oven at 40 °C, for six hours. Under the synthesis of PANI/NPG composite, aniline was polymerized by in-situ polymerization using a mixture of graphite, persulfate ions and hydrochloric acid solution. The anticorrosive coating was prepared by mixing PANI/NPG composite with xylene and alkyd resin to coat the mild steel surface [12].

<H2>2.3 Characterization

The prepared composite materials were characterized using X-ray powder diffraction (XRD) (Rigaku-Ultima IV X-ray diffractometer) with a step size 0.02° min⁻¹ and Cu K_{α1} radiation of wavelength $\lambda=0.15405$ nm, to study the interlayer expansion and to evaluate the oxidation process of graphite. The Debye-Scherrer equation was applied to the major XRD peaks of graphite and PANI/graphite in order to determine the average crystallite size of the composite. The X-ray diffractograms were analyzed using the X Powder12 software with the help of the ICDDPDF2 database. The IR spectra were obtained using Nicolet-6700, Fourier transform infrared (FTIR) spectrophotometer with attenuated total reflectance (ATR). The morphology was examined by scanning electron microscopy (SEM) equipped with energy dispersive X-ray spectroscopy (EDS) (EEVO/LS 15 ZEISS) and Hitachi S4700 with the accelerating voltage of 10 kV. The high-resolution images of periodic structures were analyzed and filtered by the fast Fourier transformation (FFT) method. The elemental composition of the material surface was studied by PHI 5000 X-ray photoelectron spectroscopy (XPS) with Al-Mg anode. Thermogravimetric analysis (TGA) and differential thermal analysis (DTA) were conducted using Shimadzu DTG 60H, at a heating rate of 10 °C min⁻¹, in an air flow, in the temperature range of 0 - 900°C. Cyclic voltammetry (CV) and linear sweep voltammetry (LSV) were performed in a three-electrode configuration cell comprising of an Ag/AgCl reference electrode, a working electrode, and a platinum gauze counter electrode using an automatic polarization system (HSV-110). CVs of the sample, deposited on FTO glass as the working electrode, were obtained in the potential domain from -0.2 to + 0.7 V, at a scan rate of 10 mV s⁻¹, in a N₂-purged 0.1 M HCl (aq) electrolyte solution. LSVs of the coated and uncoated steel rods, separately used as the working electrode, were carried in an N₂ purged 0.1 M KCl electrolyte solution in the potential range from -1.0 to +1.0 V, at a scan rate of 10 mV s⁻¹. The electrodes were dried in vacuum before the measurements. A Micro-Raman spectroscopic analysis was performed with Jasco NRS 3100 equipped with the gratings of 1800 lines/mm and CCD-detector at 10 - 30 s rate, in the first order region (1000 - 1800 cm⁻¹).

<H2>2.4 Anticorrosive studies on PANI/graphite composite coatings on mild steel surfaces

1.25 g of PANI/NPG composite material was dispersed in a mixture of an alkyd resin (2.50 g) and xylene (2.50 g) to prepare the composite coating. Also, individual

coatings of NPG, PANI, and alkyd resin were prepared by following the same procedure for comparison. These coatings were applied on a cleaned mild steel surface for the anticorrosive studies.

<H1>2. Results and Discussion

As described in the experimental section, the PANI appeared as a thick and brown color colloidal at the initial stage of polymerization of the PANI [12, 21]. The appearance of this color is most likely due to the formation of short chains of polymers or oligomers, as this is the primitive nature at the initial stage of polymerization[21]. The elongation of the polymerization results in the formation of long polymer chains, and, at the final stage, the polyaniline appeared in dark blue-green color, which is known as the color of emeraldine salt form of PANI.

The integrity of the lattice structure can be ascertained from the position of the peaks in XRD pattern. As shown in Figure 1a, the NPG has sharp distinct peaks at 2θ values of 26.54° , 55.34° and 87.66° , (JCPDS no. 23-64) corresponding to the d-spacing of 3.35, 1.67 and 1.11 Å, respectively[1]. The peak at $2\theta = 26.54^\circ$ corresponds to the (002) plane of the graphite [1, 22]. The XRD patterns of the NPG and the PANI/NPG composite provide information on the change of the crystal structure of graphite due to the formation of thin cover of PANI around NPG graphite particles [1].

Slight changes, such as the shift of the peak positions and peak broadening, have been observed for the (002) plane of graphite [1]. The average crystallite size, calculated by Debye-Scherrer formula using the major XRD peak of NPG graphite at $2\theta = 26.54^\circ$, is to be 44.8 nm. However, the average crystallite size of NPG graphite in the PANI/NPG composite is 21.6 nm and it is half less than that of the crystallite size of graphite [12]. Therefore, it suggested that the PANI discourage the aggregation of the graphite particles during the polymerization process and the PANI/NPG composites form preferably finer nano scale particles. These XRD results show the ability to synthesize PANI-graphite composite using polyaniline as the polymeric matrix.

The Fourier transform infrared (FTIR) spectrum of NPG (Figure 2a) shows the IR absorption peak around 674 cm^{-1} , which represents the bending aromatic C-H bond. The peak at 1642 cm^{-1} reveals the presence of stretching band of aromatic C=C in the graphite lattice. According to the hybridization present in the graphite, a doubly splitting peak is resulted around $2300\text{ -}2400\text{ cm}^{-1}$, which is related to stretching vibrations of sp^3 and sp^2 hybridization of C-H bonds [23, 24].

FTIR spectrum of bare PANI (Figure 2b) shows the existence of broad and strong absorption peaks in the range of $3550\text{ -}3200\text{ cm}^{-1}$, which belong to O-H stretching bond of H_2O , alcohol or phenol. These bonds are present in PANI and also in PANI/NPG composite materials as a result of the synthesis process. A medium weak single absorption peak around 3300 cm^{-1} confirms the presence of N-H stretching bond present in the prepared PANI sample. Interestingly, the amine stretching, N-H stretching, peak of the PANI/NPG composite (Figure 2c) material is near the band at 3400 cm^{-1} . Compared to the N-H stretching peak of PANI, the peak observed on the PANI/NPG composite has been slightly shifted to a higher wavenumber due to the formation of new bonds with the graphite structure. Further, peaks around 1575 and 1519 cm^{-1} show the asymmetric or symmetric stretching vibrations of C=C bonds. The multiple peaks appeared around 1485 cm^{-1} are due to benzene structure present in both PANI and PANI/NPG composite material. The peaks of C-H bending vibration in-plane or out of the plane, C-N stretching of secondary aromatic amine

are observed in the absorption range of $1138 - 834 \text{ cm}^{-1}$ and 1310 cm^{-1} , respectively. The IR spectra of NPG, PANI, and PANI/NPG composite reveal the existence of the combination of both corresponding PANI and NPG phases in the prepared composite material [25, 26].

The SEM micrographs (Figure 3) illustrate the change in graphite surface during the *in-situ* polymerization of aniline. The micrographs indicate graphite with very smooth surfaces and sharp edges, as shown in Figure 3a, and Figure 3b illustrates the distinct layered structure of NPG graphite. During the polymerization of aniline to PANI, PANI particles form worm-like agglomerated structures, which have very smooth surfaces and edges as shown in Figure 3c and d. Compared to the NPG, PANI/NPG composite, which is shown in Figure 3e and f, has an uneven surface with the graphite edges became blunted. Also, the surface of the graphite is fully covered with the PANI. Furthermore, during the polymerization, the graphite particles may have supplied some active sites to start a nucleation process of PANI [15, 26-28].

Hence, the graphite particles seems to be covered during the polymerization process. Further, an interesting feature of this process was that the layered structure of graphite could be preserved in the prepared PANI/NPG composite, as confirmed by XRD results. This happened with the help of PANI, to be successfully formed into a composite with graphite. The graphite particles have been successfully dispersed to form the composite with the PANI matrix, without obstructing the layered structure of graphite [29]. This is further confirmed by transmission electron microscopy (TEM) observations.

The TEM images of PANI and PANI/NPG are shown in Figure 4a and b, respectively. Figure 4a represents the typical TEM image of PANI nanoparticles, with a particles size ranging from 50 to 75 nm, as also reported elsewhere [21, 27]. The corresponding selected area electron diffraction (SAED) pattern shows blurred and diffused rings, which indicate that the PANI has an amorphous structure.

Interestingly, NPG has preserved its layered structure and the crystallinity during polymerization, as demonstrated in Figure 4b. Firstly, lattice fringes, as in periodic contrast, can be seen where the spacing was measured to be 0.35 nm contributing to the (001) plane of NPG [30]. Secondly, the coexistence of the PANI and NPG can be visualized by applying Fast Fourier Transform (FFT) algorithm. For example, FFs of the region 1 and 2 show distinct spots with diffuse rings. On the contrary, pure PANI appears in the region 3. Hence, it is confirmed that the surface of the NPG has been fully covered with the PANI coating while graphite maintaining its crystalline nature [16, 31].

The thermal properties of the prepared composite and NPG graphite were investigated by DTA and TGA. To determine the relative mass percentage of the composite material, thermograms were obtained, as shown in Figure 5. The TGA plot of graphite (Figure 5a) shows an 80.6 % of weight loss after $750 \text{ }^\circ\text{C}$. The drastic drop in TGA of graphite corresponds to the combustion of carbon [2]. At the same temperature region, the DTA curve of graphite demonstrates a very high endothermic reaction with a heat loss of $155 \text{ } \mu\text{V}$ at $850 \text{ }^\circ\text{C}$ [6]. In contrast, PANI shows (Figure 5b) rather different behavior in TGA and DTA. In the case of PANI, there can be seen two stage of weight losses. The first weight loss of 19.5 % at 105°C is probably due to evaporation of physisorbed water molecules[2]. The second weight loss of 76.1 % up to $636 \text{ }^\circ\text{C}$ can be attributed to the degradation of the unsaturated groups present in the polymer, whereas the PANI is stable up to $636 \text{ }^\circ\text{C}$ [2, 6].

The DTA curve of pure PANI exhibits an endothermic peak at 107 °C, due to the dehydration (loss of water). The last endothermic peak at 396 °C can be ascribed to its decomposition [6]. Interestingly, the TGA plot of the PANI/NPG composite illustrated in fig. 5c reveals the weight loss of 42 % in the temperature range from 81 to 545 °C, which is specified to the thermal decomposition of PANI [1, 11]. The TGA weight loss of 66 % in the temperature range of 545 to 850 °C is attributed to the decomposition of the graphite component [1]. The TGA information is further supported by the DTA profile of the composite material. The DTA curve of PANI/NPG composite demonstrates two endothermic reaction at 395 and 750 °C, which corresponds to the decomposition of PANI and NPG respectively [1, 6, 32]. As in Figure 5, the TGA and DTA curves of PANI/NPG composite established the presence of both NPG and PANI in the composite, with the mass ratio of approximately 3 to 2 in the case of 66 % NPG to 42 % PANI.

Raman spectroscopy was employed to study the structure, defect levels and crystallinity of the NPG and PANI/NPG composite. The micro-Raman spectrum of NPG shown in Figure 6a shows G and 2D bands at 1577.9 and 2710.8 cm^{-1} , respectively [29, 33]. The Raman shift of G band is due to the first-order scattering of the E_{2g} phonon of sp^2 carbon present in graphite lattice and the 2D band is associated with the particular stacking order of graphite along the c-axis. It was reported that 2D peak is observed at twice of the wavelength of the D band (1343.6 cm^{-1}), and the 2D peak can be observed either presence or absence of the D peak [24, 29]. On the spectrum of NPG, shown in Figure 5a, very weak D band with very low intensity can be observed. This could explain from the structural point of view where the D band intensity is associated with the grain size and distortions at the edge of graphite, tabulated in Table 1. Therefore, it can be concluded that the purified and surface modified NPG has negligible edge distortions, may be due to the stirring process during the purification process [24, 29, 33].

The Raman spectrum of PANI exhibits the patterns of emeraldine structure[34]. The peaks assigned to functional groups of PANI were found at 1190 cm^{-1} (C-H bending of benzenoid ring), 1490 cm^{-1} (C-N stretching of benzenoid ring), 1510 cm^{-1} (C=N stretching of quinoid ring), 1580 cm^{-1} (C=C stretching of quinoid ring) and 1650 cm^{-1} (C-C stretching of the benzenoid ring) [27, 33, 34]. The existence of these functional groups in PANI was also confirmed by the FTIR transmittance spectrum shown in Figure 2b. Interestingly, the spectrum of the PANI/NPG composite (Figure 6c) clearly illustrate the combination of both NPG and PANI associated with the composite structure. The spectrum reveals the very low level of defects formation at the edge of the NPG during the polymerization of PANI, may resulted from the stirring during forming this composite material. However, PANI/NPG composite can also be formed with this *in-situ* chemical synthesis process, with a minimum level of distortion to the crystallinity of the NPG. The XRD analysis of PANI/NPG reported previously, also confirmed the preservation of the crystalline structure of NPG after the polymerization process, which is consistent with STM images.

The XPS measurements of NPG, PANI and PANI/NPG were performed to gather information about their composition, the degree of polymerization and the type of present oxygen species. The XPS survey spectra and de-convoluted C1s core level spectra of NPG, PANI and PANI/NPG are presented in Figure 7 and Figure 8, respectively. Survey spectra show C1s, and O1s peaks in all the three samples and N1s peak was observed in the spectra of PANI and PANI/NPG composite. The presence of strong O1s in NPG is due to physically absorbed oxygen [33]. To identify the different oxygen functional groups that formed on the basal or edge plane

of carbon, high-resolution C1s core level spectra of NPG, PANI and PANI/NPG were observed. As expected, in fig. 8a, the high purity NPG graphite displays a prominent peak at a binding energy (B.E) of 284.4 eV from the sp^2 carbon in graphite [33]. Further, at a binding energy (B.E) of 284.6 and 285.3 eV, the characteristic peaks of C-C sp^3 and hydroxyl (C-OH) were exhibited [7, 33, 34].

The de-convoluted C1s core level spectra of PANI (Figure 8b) represent characteristic peaks of C-C sp^2 , C-C sp^3 , hydroxyl (C-OH), and amine (C-N) in the B.E of 284.3, 284.7, 287.1, and 285.8 eV respectively [33, 35]. Furthermore, the presence of the same bond presented in PANI/NPG composite is confirmed in the freshly prepared composite material. Interestingly, specific oxygen functional groups determined by FTIR analysis (Figure 2) of the three samples mentioned above is consistent with XPS analysis results.

Figure 9 shows the CVs of PANI and PANI/NPG composite on bare FTO glass, which was used as the electrode substrate, in 0.1 M HCl solution[4, 36]. The CVs of PANI shows two oxidation states, P_1 at +0.12 V and P_2 at +0.40 V, and two reduction peaks, P_1' at -0.09 V and P_2' at +0.33 V, existing due to the formation of three states of PANI known as leucomeraldine, emeraldine and pernigraniline. It is expected that, P_1 is due to the oxidation of pernigraniline to emeraldine salt form, and P_2 is further oxidation of emeraldine to leucomeraldine. Considering the reduction process, P_2' corresponds to the reduction of leucomeraldine to emeraldine salt form and P_1' is due to further reduction of emeraldine into pernigraniline. This redox processes of PANI is almost reversible and it reveals (Figure 9a) the formation of emeraldine salt form and then converting to the leucoemeraldine salt form [12, 28]. Interestingly, the higher current observed at a higher potential than 0.7 V for PANI is due to oxidation (or dissolution) of the electrode. In addition, CV of PANI/NPG reveals suppression of the reaction (oxidation or dissolution) on the PANI/NPG covered surface. In contrast, the leucomeraldine salt has been spontaneously converted back to the emeraldine salt form due to the contact of atmospheric oxygen with the coating [12, 13]. The redox behavior of PANI and the PANI/NPG composite with high reproducibility suggests high stability of the coating membrane. Further, CV with the higher scan rate demonstrates the disappearance of the redox peaks, due to the inadequate time for the ionic transportation [27, 36].

The specific capacity of PANI/NPG was calculated according to the following equation: [36]

$$C = \int_{E_2}^{E_1} i(E) dE / (2v / (E_2 - E_1))$$

where C is capacitance (in farad (F)), $i(E)$ is the instantaneous current (in A), $\int i(E) dE$ is the total charge obtained by integration of positive and negative sweep in CV

(10 mV s⁻¹) except faradic peaks portion (in A.V). (E2-E1) is the potential window width (in V), and ν is scan rate (in V s⁻¹) [14, 35, 36].

It is noted that the specific capacitance, 833.3F g⁻¹ of PANI/NPG composite is higher than 484.5 F g⁻¹ of the pure PANI, at the same scan rate[30, 36]. This synergism resulted in good electrochemical performance between PANI and NPG [12, 36, 37].

The Tafel plot of mild steel electrodes with different coatings is shown in Figure 10.

The details of the coatings used and electrochemical parameters are tabulated in Table 2. According to the Table 2 and the Tafel plot, the corrosion rate is the largest for the bare steel rod, on which the annual corrosion rate is 23210 μm per year.

Taking this as a reference and assigning the percentage as 100%, the corrosion rates of all materials were calculated as percentage corrosion rate, $R_M\%$, (Table 2). In contrast to the bare steel rod, a corrosion rate of 15.85% was observed for the alkyd resin.

Further, the Tafel plot for the alkyd resin shows a significant change for corrosion with an E_{corr} of -0.63 V. When NPG/PANI coating is used, the relative corrosion rate is further reduced to 0.12%, and it is much lower than that of NPG and PANI [12, 16]. This clearly demonstrates the ability of the PANI/NPG composite to work as a barrier to avoid the penetration of O₂ or H₂O towards the steel surface.

Moreover, the positive corrosion potential of the prepared composite material elucidates its high stability, compared to PANI and NPG, individually. This high positive potential of PANI and PANI/NPG is due to the formation of the specific passive layer between steel surface and the coating material by adsorption of the polymer and graphite on the steel surface and/or complexation of Fe and PANI.

The corrosion potential of PANI (+0.26 V) is lower than that of PANI/NPG (+0.55 V) composite while steel has the lowest corrosion potential as -0.72 V in all test-samples. The improvement of corrosion protection effect on the PANI/NPG coating steel rods should be a result of well-dispersion of the NPG graphite in the PANI matrix where tortuosity of diffusion pathways for oxygen and water vapor is increased [38, 39]. The corrosion and rust formation on steel involves different processes in the solution with and without O₂ medium as shown in the following equation (a) and (b):

<remove picture pageno 11>with O₂; Fe (s) + H₂O (l) + 1/2 O₂ (g) Fe²⁺ (aq) + 2 OH⁻

(aq) (a)

<remove picture pageno 11>without O₂; Fe (s) + 2 H⁺ (aq) Fe²⁺ (aq) + H₂(g) or; (b)

<remove picture pageno 11>Fe (s) + 2 H₂O (l) Fe²⁺ (aq) + H₂ (g) + 2OH⁻ (aq)

The equation indicates that sufficient amount of H₂O and O₂ are required for the formation of rust and dissolution of the steel for causing corrosion. If any of these processes are prevented, the corrosion is inhibited and the coating provides effective corrosion prevention. The combination of layered structure of the NPG graphite and the long chain carbon structure of PANI in the PANI/NPG composite greatly supports to increase the tortuosity to prevent the corrosion than the case of applying the NPG and PANI separately as the coating. Therefore, our results reveal that increasing the tortuosity of the diffusion pathways is able to effectively prevent the H₂O and O₂ from accessing the substrate surface, leading a good anticorrosion property [18, 39]. It is noteworthy that the corrosion potential of the PANI and PANI/NPG composite coating samples was shifted negative, -0.56 and -0.35 V, under O₂ purge condition, where O₂ partial pressure was increased. It suggests that presence and amount of H₂O and O₂ is important factor for the corrosion.

Figure 11 shows the contact angle measurements of NPG, PANI, PANI/NPG composite and alkyd resin coatings on metal surfaces. Interestingly, the PANI/NPG composite coating has the highest contact angle of 117.9° compared to PANI and NPG separately, while the bare NPG and PANI itself also have a good hydrophobicity. With the formation of the PANI/NPG composite material, hydrophobicity or the contact angle on the coating steel surfaces have been increased. This can help to develop a good adhesion with the metal surface and prevent the corrosion of the metal surface.

Carbon-based surfaces widely exist for both nanoscale as well as for macroscopic materials macroscopic materials. Most of these carbon-based surfaces, such as of graphite, contain a graphitic surface composed of aromatic rings, which are hexagonal carbon rings rich in π electrons [40]. An aromatic ring is composed of relatively non-polar C-C and C-H bonds, which is confirmed by the FTIR analysis presented in Figure 2, are not effectively solvated by water. In contrast, the electronegativity difference between C and H is rather small, and that between C and C is zero. There is thus no charge separation on the benzene ring hence no polarity, which would lend itself to solvation by the polar water. Therefore, It is well recognized that most of these graphitic surfaces, rich in aromatic rings are hydrophobic similar to those of graphite, can result in contact angle such as 106.4° with water.

In other words, considering the structure of PANI, it contains a lot of hydroxyl (-OH), amine (-NH), and benzene rings [41, 42]. According to literature, because of the hydrophilic -OH and -NH groups and the hydrophobic benzene rings, the contact angle for PANI is decreasing to 93.5° compared to graphite. But still, it's hydrophobic due to the presence of higher amount of hydrophobic groups than the hydrophilic groups in PANI structure.

The contact angle of the composite has become 117.9° which is higher than that of both PANI and Graphite. This composite material is composed of both the NPG graphite and PANI. In this resultant PANI/NPG composite, the amount of NPG is larger than that of PANI presence in the composite. Therefore, a number of hydrophobic aromatic rings contributing to the final structure are very large than the contribution from hydroxyl (-OH) and amine (-NH) groups from PANI to the final structure of this PANI/NPG composite. Therefore, PANI/NPG composite has become more hydrophobic than the PANI and NPG itself.

<H1>4 Conclusion

PANI/graphite composite material was synthesized by using natural NPG vein graphite. It is found that the composite works as an anti-corrosive coating on steel surfaces. In addition, the prepared composite shows good hydrophobic ability, which is very useful in preventing corrosion on metal surfaces caused by oxygen penetration towards the metal surface. Furthermore, the PANI/graphite composite is a highly thermal stable material which shows a heat resistance up to 700°C . These results suggest that the PANI/NPG composite is a suitable and promising material for high-tech applications, such as surface coating and electrode for batteries. The prepared PANI/NPG composite material shows a significantly high corrosion resistance compared to alkyd resin/PANI coatings or alkyd resin coatings, on steel surfaces.

Altogether, this study reveals the successful synthesis of PANI/NPG composite with polyaniline and naturally occurring NPG vein graphite. It further indicted the capability of this PANI/NPG composite as a highly hydrophobic, anticorrosive and low cost surface coating material for steel surfaces.

<REF>References

<BIBL>

- [1] S.E. Bourdo, B.A. Warford, T. Viswanathan,;1; Electrical and thermal properties of graphite/polyaniline composites, *Journal of Solid State Chemistry*, 196 (2012) 309-313.
- [2] B.R. Hsieh, Y. Wei,;1; *Semiconducting Polymers*, American Chemical Society, 1999.
- [3] B. Veeraraghavan, J. Paul, B. Haran, B. Popov,;1; Study of polypyrrole graphite composite as anode material for secondary lithium-ion batteries, *Journal of Power Sources*, 109 (2002) 377-387.
- [4] H. Karami, M.F. Mousavi, M. Shamsipur,;1; A new design for dry polyaniline rechargeable batteries, *Journal of Power Sources*, 117 (2003) 255-259.
- [5] S.E. Bourdo, T. Viswanathan,;1; Graphite/Polyaniline (GP) composites: Synthesis and characterization, *Carbon*, 43 (2005) 2983-2988.
- [6] C. Yang, Z. Fang, J. Liu, W. Liu, H. Zhou,;1; A study on the kinetics of thermal decomposition of polyaniline, *Thermochimica Acta*, 352–353 (2000) 159-164.
- [7] R.M.N.M. Rathnayake, H.W.M.A.C. Wijayasinghe, H.M.T.G.A. Pitawala, M. Yoshimura, H.-H. Huang,;1; Synthesis of graphene oxide and reduced graphene oxide by needle platy natural vein graphite, *Applied Surface Science*, 393 (2017) 309-315.
- [8] Y. Li, X. Zhao, P. Yu, Q. Zhang,;1; Oriented Arrays of Polyaniline Nanorods Grown on Graphite Nanosheets for an Electrochemical Supercapacitor, *Langmuir*, 29 (2013) 493-500.
- [9] L.-M. Huang, C.-H. Chen, T.-C. Wen,;1; Development and characterization of flexible electrochromic devices based on polyaniline and poly(3,4-ethylenedioxythiophene)-poly(styrene sulfonic acid), *Electrochimica Acta*, 51 (2006) 5858-5863.
- [10] J. Stejskal, I. Sapurina, M. Trchová, J. Prokeš, I. Křivka, E. Tobolková,;1; Solid-State Protonation and Electrical Conductivity of Polyaniline, *Macromolecules*, 31 (1998) 2218-2222.
- [11] B.Z. Tang, Y. Geng, J.W.Y. Lam, B. Li, X. Jing, X. Wang, F. Wang, A.B. Pakhomov, X.X. Zhang,;1; Processible Nanostructured Materials with Electrical Conductivity and Magnetic Susceptibility: Preparation and Properties of Maghemite/Polyaniline Nanocomposite Films, *Chemistry of Materials*, 11 (1999) 1581-1589.
- [12] K.G.C. Senarathna, M.M.M.G.P.G. Mantilaka, T.A.N. Peiris, H.M.T.G.A. Pitawala, D.G.G.P. Karunaratne, R.M.G. Rajapakse,;1; Convenient routes to synthesize uncommon vaterite nanoparticles and the nanocomposites of alkyd resin/polyaniline/vaterite: The latter possessing superior anticorrosive performance on mild steel surfaces, *Electrochimica Acta*, 117 (2014) 460-469.
- [13] L. Zhong, H. Zhu, J. Hu, S. Xiao, F. Gan,;1; A passivation mechanism of doped polyaniline on 410 stainless steel in deaerated H₂SO₄ solution, *Electrochimica Acta*, 51 (2006) 5494-5501.
- [14] V. Gnedenkov Sergey, P. Sharkeev Yurii, L. Sinebryukhov Sergey, A. Khrisanova Olga, V. Legostaeva Elena, G. Zavidnaya Alexandra, V. Puz' Artem, A. Khlusov Igor, P. Opra Denis,;1; Functional coatings formed on the titanium and

magnesium alloys as implant materials by plasma electrolytic oxidation technology: fundamental principles and synthesis conditions, in: *Corrosion Reviews*, 2016, pp. 65.

- [15] P. Sambyal, G. Ruhi, R. Dhawan, S.K. Dhawan,;1; Designing of smart coatings of conducting polymer poly(aniline-co-phenetidine)/SiO₂ composites for corrosion protection in marine environment, *Surface and Coatings Technology*, 303, Part B (2016) 362-371.
- [16] G. Ruhi, O.P. Modi, S.K. Dhawan,;1; Chitosan-polypyrrole-SiO₂ composite coatings with advanced anticorrosive properties, *Synthetic Metals*, 200 (2015) 24-39.
- [17] P. Touzain, N. Balasooriya, K. Bandaranayake, C. Descolas-Gros,;1; VEIN GRAPHITE FROM THE BOGALA AND KAHATAGAHA–KOLONGAHA MINES, SRI LANKA: A POSSIBLE ORIGIN, *The Canadian Mineralogist*, 48 (2010) 1373-1384.
- [18] Y.-H. Yu, Y.-Y. Lin, C.-H. Lin, C.-C. Chan, Y.-C. Huang,;1; High-performance polystyrene/graphene-based nanocomposites with excellent anti-corrosion properties, *Polymer Chemistry*, 5 (2014) 535-550.
- [19] J.-M. Yeh, S.-J. Liou, C.-Y. Lai, P.-C. Wu, T.-Y. Tsai,;1; Enhancement of Corrosion Protection Effect in Polyaniline via the Formation of Polyaniline–Clay Nanocomposite Materials, *Chemistry of Materials*, 13 (2001) 1131-1136.
- [20] J. Xu, Y. Hu, L. Song, Q. Wang, W. Fan,;1; Preparation and characterization of polyacrylamide-intercalated graphite oxide, *Materials Research Bulletin*, 36 (2001) 1833-1836.
- [21] B.A. Bhanvase, S.H. Sonawane,;1; New approach for simultaneous enhancement of anticorrosive and mechanical properties of coatings: Application of water repellent nano CaCO₃–PANI emulsion nanocomposite in alkyd resin, *Chemical Engineering Journal*, 156 (2010) 177-183.
- [22] Z.Q. Li, C.J. Lu, Z.P. Xia, Y. Zhou, Z. Luo,;1; X-ray diffraction patterns of graphite and turbostratic carbon, *Carbon*, 45 (2007) 1686-1695.
- [23] G. Venkata Ramana, B. Padya, V.V.S.S. Srikanth, P.K. Jain, G. Padmanabham, G. Sundararajan,;1; Electrically conductive carbon nanopipe-graphite nanosheet/polyaniline composites, *Carbon*, 49 (2011) 5239-5245.
- [24] E.-Y. Choi, T.H. Han, J. Hong, J.E. Kim, S.H. Lee, H.W. Kim, S.O. Kim,;1; Noncovalent functionalization of graphene with end-functional polymers, *Journal of Materials Chemistry*, 20 (2010) 1907-1912.
- [25] I.A. Tchmutin, A.T. Ponomarenko, E.P. Krinichnaya, G.I. Kozub, O.N. Efimov,;1; Electrical properties of composites based on conjugated polymers and conductive fillers, *Carbon*, 41 (2003) 1391-1395.
- [26] J.L. Gutiérrez-Díaz, J. Uruchurtu-Chavarín, M. Güizado-Rodríguez, V. Barba,;1; Steel protection of two composite coatings: Polythiophene with ash or MCM-41 particles containing iron(III) nitrate as inhibitor in chloride media, *Progress in Organic Coatings*, 95 (2016) 127-135.
- [27] J. Yan, T. Wei, B. Shao, Z. Fan, W. Qian, M. Zhang, F. Wei,;1; Preparation of a graphene nanosheet/polyaniline composite with high specific capacitance, *Carbon*, 48 (2010) 487-493.
- [28] J. Kim, S. Kim,;1; Preparation and electrochemical analysis of graphene/polyaniline composites prepared by aniline polymerization, *Research on Chemical Intermediates*, 40 (2014) 2519-2525.
- [29] J.S.Y. Chia, M.T.T. Tan, P. SimKhiew, J.K. Chin, H. Lee, D.C.S. Bien, A. Teh, C.W. Siong,;1; Facile synthesis of few-layer graphene by mild solvent thermal exfoliation of highly oriented pyrolytic graphite, *Chemical Engineering Journal*, 231 (2013) 1-11.

- [30] A. Adhikari, P. Claesson, J. Pan, C. Leygraf, A. Dédinaité, E. Blomberg,;1; Electrochemical behavior and anticorrosion properties of modified polyaniline dispersed in polyvinylacetate coating on carbon steel, *Electrochimica Acta*, 53 (2008) 4239-4247.
- [31] N. Sarkar, G. Sahoo, R. Das, G. Prusty, D. Sahu, S.K. Swain,;1; Anticorrosion Performance of Three-Dimensional Hierarchical PANI@BN Nanohybrids, *Industrial & Engineering Chemistry Research*, 55 (2016) 2921-2931.
- [32] M. Rodas, F.J. Luque, J.F. Barrenechea, J.C. Fernández-Caliani, A. Miras, C. Fernández-Rodríguez,;1; Graphite occurrences in the low-pressure/high-temperature metamorphic belt of the Sierra de Aracena (southern Iberian Massif), in: *Mineralogical Magazine*, 2000, pp. 801.
- [33] P. Dash, T. Dash, T.K. Rout, A.K. Sahu, S.K. Biswal, B.K. Mishra,;1; Preparation of graphene oxide by dry planetary ball milling process from natural graphite, *RSC Advances*, 6 (2016) 12657-12668.
- [34] M. Sawangphruk, M. Suksomboon, K. Kongsupornsak, J. Khuntilo, P. Srimuk, Y. Sanguansak, P. Klunbud, P. Suktha, P. Chiochan,;1; High-performance supercapacitors based on silver nanoparticle-polyaniline-graphene nanocomposites coated on flexible carbon fiber paper, *Journal of Materials Chemistry A*, 1 (2013) 9630-9636.
- [35] E. Binkauskienė, V. Jasulaitienė, A. Lugauskas,;1; Effect of *Aspergillus niger* Tiegh. L-10 on the physical and chemical properties of a polyaniline coating in the growth substrate, *Synthetic Metals*, 159 (2009) 1365-1368.
- [36] Q. Zhang, Y. Li, Y. Feng, W. Feng,;1; Electropolymerization of graphene oxide/polyaniline composite for high-performance supercapacitor, *Electrochimica Acta*, 90 (2013) 95-100.
- [37] H. Zhang, G. Cao, W. Wang, K. Yuan, B. Xu, W. Zhang, J. Cheng, Y. Yang,;1; Influence of microstructure on the capacitive performance of polyaniline/carbon nanotube array composite electrodes, *Electrochimica Acta*, 54 (2009) 1153-1159.
- [38] K. Cai, S. Zuo, S. Luo, C. Yao, W. Liu, J. Ma, H. Mao, Z. Li,;1; Preparation of polyaniline/graphene composites with excellent anti-corrosion properties and their application in waterborne polyurethane anticorrosive coatings, *RSC Advances*, 6 (2016) 95965-95972.
- [39] C.-H. Chang, T.-C. Huang, C.-W. Peng, T.-C. Yeh, H.-I. Lu, W.-I. Hung, C.-J. Weng, T.-I. Yang, J.-M. Yeh,;1; Novel anticorrosion coatings prepared from polyaniline/graphene composites, *Carbon*, 50 (2012) 5044-5051.
- [40] Z. Li, Y. Wang, A. Kozbial, G. Shenoy, F. Zhou, R. McGinley, P. Ireland, B. Morganstein, A. Kunkel, S.P. Surwade, L. Li, H. Liu,;1; Effect of airborne contaminants on the wettability of supported graphene and graphite, *Nat Mater*, 12 (2013) 925-931.
- [41] H. Ding, C. Zhu, Z. Zhou, M. Wan, Y. Wei,;1; Hydrophobicity of Polyaniline Microspheres Deposited on a Glass Substrate, *Macromolecular Rapid Communications*, 27 (2006) 1029-1034.
- [42] C. Zhou, X. Gong, Y. Qu, J. Han,;1; Hydrophobic and high adhesive polyaniline layer of rectangular microtubes fabricated by a modified interfacial polymerization, *Applied Surface Science*, 379 (2016) 124-131.

</BIBL>

<Figure>Figure 1. X-ray diffractograms of (a) NPG graphite and (b) PANI/NPG composite

<Figure>Figure 2. FTIR spectra of (a) NPG, (b) PANI and (c) PANI/NPG composite

<Figure>Figure 3. SEM micrographs of NPG (a, b), PANI (c, d) and PANI/NPG (e, f) composite.

<Figure>Figure 4. Low-magnification bright-field TEM images of (a) PANI, and (b) PANI/NPG composite with inset of corresponding diffraction patterns along the [100] zone axis

<Figure>Figure 5. TGA/DTA curves of (a) NPG, (b) PANI and (c) PANI/NPG composite

<Figure>Figure 6. Micro-Raman spectra of (a) NPG, (b) PANI and (c) PANI/NPG composite

<Figure>Figure 7. XPS survey spectra of (a) NPG, (b) PANI and (c) PANI/NPG

<Figure>Figure 8. De-convoluted C1s spectra of (a) NPG, (b) PANI and (c) PANI/NPG

<Figure>Figure 9. Cyclic voltammograms of (a) PANI and (b) PANI/NPG graphite composite in 0.1 M HCl solution. Scan rate is 10 mV s⁻¹

<Figure>Figure 10. The Tafel plots for (a) bare steel (b) alkyd-resin, (c) NPG, (d) PANI and (e) PANI/NPG composite, on steel rods.

<Figure>Figure 11. Photo images of contact angle measurements of (a) NPG, (b) PANI, (c) Alkyd resin and (d) PANI/NPG

<Table>Table 1. Calculation of I_D/I_G ratio values from micro Raman spectra of NPG, PANI and PANI/NPG composite

Sample ID	D peak, (cm ⁻¹)	G peak, (cm ⁻¹)	2D peak, (cm ⁻¹)	I _D	I _G	I _D /I _G
NPG	1343.6	1577.9	2721.8	3.6	14344.6	~0
PANI	-	-	-	-	-	-
PANI/NPG	1166.7	1573.4	2693.8	720.4	3553.0	0.2

<Table>Table 2. Corrosion rate calculation for prepared coating on metal rod

Electrochemical corrosion studies				
Coating	E_{corr}/ V	J_{corr}/A cm⁻²	R_M/ μm yer⁻¹	R_M %
PANI/NPG	+0.55	2.5 x 10 ⁻⁶	29	0.12
PANI	+0.26	3.2 x 10 ⁻⁶	36	0.16
NPG	-0.55	2.0 x 10 ⁻⁴	2320	9.99
Alkyd Resin	-0.63	3.2 x 10 ⁻⁴	3680	15.85
Bare Steel	-0.72	2.0 x 10 ⁻³	23210	100

TDENDOFOCTD